JOURNAL OF THEORETICAL AND APPLIED MECHANICS
61, 2, pp. 355-364, Warsaw 2023
https://doi.org/10.15632/jtam-pl/163053

IMPLEMENTATION OF A VISCOELASTIC BOUNDARY CONDITION TO YADE – OPEN SOURCE DEM SOFTWARE

Karol Brzeziński, Artur Zbiciak
Warsaw University of Technology, Faculty of Civil Engineering, Warsaw, Poland
e-mai: karol.brzezinski@pw.edu.pl
Anton Gladky
Independent Researcher, e-mail: gladky.anton@gmail.com

The paper presents implementation of a viscoelastic boundary condition to Yade software. The implemented boundary condition constraints linear displacements of bodies by applying a reaction force resulting from a solution of the Burgers rheological model. This work presents the results of one of validation tests, where the output of Discrete Element Simulation (DEM) was compared with an analytically formulated soft-contact problem. Furthermore, potential application in more complex simulations (plate load test) is demonstrated. It shows that the proposed approach allows for realistic yet efficient modeling of foundations purely within the DEM framework.

Keywords: Discrete Element Method, viscoelastic boundary condition, granular layers, pavement subsoil

1. Introduction

The subgrade impacts pavement performance and service life (Puppala *et al.*, 2009; Saad *et al.*, 2005). Hence, it is important that pavement models can accurately reflect their behavior. The subgrade can be represented by analytical or numerical models depending on the adopted methodology. For example, the Winkler foundation (Winkler, 1867) is a simple one-dimensional analytical model. Well-known engineering software, such as VEROAD and BISAR programs (Dejong *et al.*, 1973; Hopman, 1996; Zbiciak *et al.*, 2019), utilize an analytical solution of multi-layered half-space. Nevertheless, the application of purely analytical models is limited to simple geometry and load cases. Numerical methods are more versatile. The Finite Element Method (FEM) allows for modeling of complex shapes, material properties and loading scenarios. However, the size of the FEM model needs to be limited. The Discrete Element Method (DEM), introduced by (Cundall and Strack, 1979), is a numerical approach that simulates behavior of granular assemblies by analyzing movements and interactions of individual particles. Consequently, one can study various phenomena at the microstructural level. The DEM is widely applied to simulate the behavior of pavement materials, such as soil and aggregate compaction (Brzeziński and Gladky, 2022; Chen *et al.*, 2021; Gladkyy and Kuna, 2017; Pei and Yang, 2018), asphalt mixtures compaction (Zhu *et al.*, 2022), creep (Quezada and Chazallon, 2022) and rutting (Zhang *et al.*, 2022). However, it comes with a high computational cost. That is why DEM analyses often focus on a small portion of a structure, and the granular assembly needs to be embedded by some deformable boundaries. Among various approaches, the following are often utilized:

- Outer bodies are fixed in place. However, due to their contact stiffness, such a boundary shows some resilience.

- Reaction forces can be applied to outer elements (selected or automatically detected). The force is servo-controlled based on displacement or may be adjusted to satisfy a stress criterion (e.g., membrane simulation (Cheung and O'Sullivan, 2008)).
- Some of researchers use long interactions (Itasca's Particle Flow Code Documentation 7.0, 2021) to set up a two-layered boundary (Pei and Yang, 2018). The outermost layer (e.g., bottom) is fixed in place. The inner layer is bound with external particles with long deformable interactions. The analyzed granular assembly contacts only the inner layer.
- The boundary can be created by a deformable assembly of particles simulating a steel or geosynthetic net (Cheng *et al.*, 2016; Thoeni *et al.*, 2014).
- Coupling with the FEM (Orosz and Zwierczyk, 2020; Stránsky, 2013) or Finite Difference Method (Jia *et al.*, 2021) is an even more sophisticated approach. It not only allows for creating boundary conditions for a granular assembly but also efficiently models and allows for analyzing adjacent structures.

This paper proposes an easy and efficient approach for the modeling of the foundation in DEM simulations. This simple and versatile approach is similar to the Winkler foundation – the reaction force is prescribed to the element based on displacement. However, the adopted force-displacement relationship is described by a solution of the Burgers model (Zbiciak *et al.*, 2017). Hence, it can reflect basic viscoelastic phenomena: creep and relaxation. The proposed feature was implemented in Yade (Smilauer *et al.*, 2021), a popular open-source software for DEM simulations. Such a procedure can be easily programmed as a user sub-routine (e.g., Python function in the case of Yade). Nevertheless, implementation in the source code (using C++) is more efficient and ready for use right after software installation. The Burgers model can be easily degenerated within the proposed approach to simpler models (Zener, Kelvin-Voigt, Maxwell or purely elastic) by prescribing certain values to parameters of the model. Thus, it can be used to model various boundary conditions, e.g., Winkler foundation.

The paper briefly describes implementation of the viscoelastic boundary condition to Yade software. Next, an analytical formulation of a soft-contact problem is presented, and its solution is compared with the results of the DEM simulation. Finally, the results of examplary application to an engineering problem (simulation of a plate load test) are demonstrated.

2. Methods

2.1. Viscoelastic boundary implementation

Yade software conducts DEM simulation iteratively. Generally, each iteration consists of the following steps (Smilauer *et al.*, 2021):

a) Resetting of all forces acting on bodies
b) Collision detections between the bodies
c) Computing interactions between simulated objects and their properties
d) Applying forces to the bodies, based on the assumed contact laws
e) Computing new velocities and then positions of the particles.

The implemented boundary condition is a function that can be run between steps (d) and (e). Hence, the forces acting on the particles are modified before computation of new positions. The function takes a list of Id's (unique identifiers) of the bodies that should be constrained and the viscoelastic parameters (see also Fig. 1), where: k_1 – stiffness of spring 1 (the one in the Maxwell branch) [N/m]; k_2 – stiffness of spring 2 (the one in the Kelvin-Voigt branch) [N/m]; c_1 – damping coefficient of dashpot 1 (the one in the Maxwell branch). A negative value turns off the dashpot [Ns/m]; c_2 – damping coefficient of dashpot 2 (the one in the Kelvin-Voigt branch). A negative value turns off the whole Kelvin-Voigt branch [Ns/m].

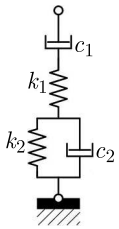

Fig. 1. Rheological scheme of the viscoelastic boundary condition

During the simulation, the initial position of the constrained body is stored in the program memory, and the current position is known from the integration conducted in the previous iteration. Thus, the model reaction can be obtained from a trivial solution to an algebraic set of equations not presented in the paper. In order to make the model more versatile, the option of dashpot deactivation was added (constraining their displacements to zero) by applying a negative value. This way, the user can switch to models simpler than the Burgers one.

2.2. Validation test – soft-contact problem

The same task was solved with two approaches to validate the proposed implementation of a viscoelastic boundary condition. First, the soft-contact problem was analytically formulated and solved with a numerical integration algorithm implemented in Python SciPy library. Next, the same issue was addressed by DEM simulation using Yade software (Smilauer *et al.*, 2021).

2.2.1. Analytical formulation

Let us consider the description of the soft-contact phenomenon in the system visualized in Fig. 2. The upper part of the model is composed of a rigid body (material point) possessing mass m_I and connected in series with a spring k_3. The lower part of the model represents linear viscoelastic boundary constraint having stiffness (spring) parameters k_1 and k_2, viscosity c_2 (damper) and equivalent mass m_{II}.

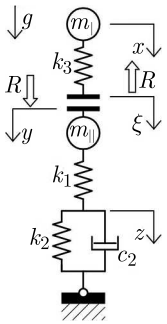

Fig. 2. Visualization of the simplified viscoelastic soft-contact model (no dashpot c_1)

The unilateral constraint between the upper and lower part of the model is visualized in Fig. 2 by two bold horizontal lines representing mass-less bumpers. The gravitational acceleration is denoted as g.

The coordinates x, ξ, y and z shown in Fig. 2 determine the displacement of material points and deformation of the rheological structure. R denotes the force of mutual interaction between the material point m_{II} and the spring k_3. The configuration shown in Fig. 2 represents such a time instant when $x = 0$ and $\xi = 0$, and $y = 0$ and $z = 0$. In the case of this configuration, both bumpers are in contact, but the spring and dashpot forces as well as the reaction R are equal to zero.

The description of the contact problem for the analyzed system may be obtained by formulation of the material points motion and evolution of the structure deformation.

The equations describing the soft-contact problem are as follows

$$\begin{aligned} &m_I\ddot{x} = m_I g - R \qquad k_3(\xi - x) = -R \\ &m_{II}\ddot{y} = m_{II} g + R - k_1(y - z) \qquad k_1(y - z) = c_2\dot{z} + k_2 z \end{aligned} \tag{2.1}$$

and

$$u = y - \xi \qquad u \geqslant 0 \qquad R(\widetilde{u} - u) \geqslant 0 \qquad \forall \widetilde{u} \geqslant 0 \tag{2.2}$$

where Eq. $(2.1)_1$ and Eq. $(2.1)_3$ describe motion of the material points m_I and m_{II}, respectively, while Eq. $(2.1)_2$ and Eq. $(2.1)_4$ represent the evolution of the structure deformation. Moreover, the system of variational inequalities (2.2) defines the relationships between the coordinate $u = y - \xi$ and the reaction R. The coordinates y and ξ denote displacements of the mass-less bumpers connected with the mass m_{II} and m_I, respectively. It can be proved that Eqs. (2.2) can be visualized via the mapping shown in Fig. 3a. (see Zbiciak and Kozyra, 2015).

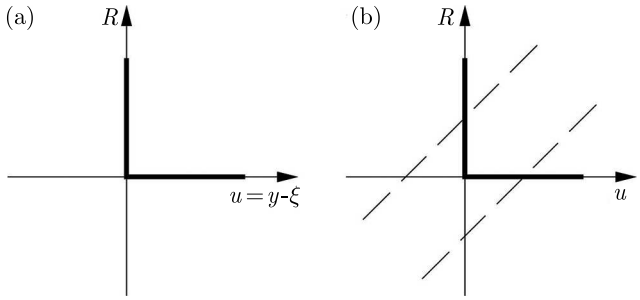

Fig. 3. Graph of the mapping expressed by Eqs. (2.2) (a) and a graphical solution leading to Eq. $(2.5)_2$ (b)

Our objective is to transform a non-linear system of Eqs. (2.1) and (2.2) to the system of explicit non-linear differential-algebraic equations (DAE). The expected system of equations should have the following form

$$\begin{aligned} &\ddot{x} = -\frac{R}{m_I} + g \qquad \ddot{y} = \frac{R}{m_{II}} - \frac{k_1}{m_{II}}(y - z) + g \\ &\dot{z} = -\frac{k_1 + k_2}{c_2} z + \frac{k_1}{c_2} y \qquad \xi = f_\xi(x, y) \qquad R = f_R(x, y) \end{aligned} \tag{2.3}$$

where Eqs. $(2.3)_{1,2,3}$ can be easily obtained using Eqs. $(2.1)_1, 3, 4$, respectively.

Let us find the functions f_ξ and f_R describing time histories of the displacement ξ and reaction R, respectively. To do so, Eq. $(2.1)_2$ should be re-written in the following equivalent form

$$R = k_3(y - \xi) + k_3(x - y) \tag{2.4}$$

Above Eq. (2.4) is a linear relation between R and $u := y - \xi$. Thus, using Eq. (2.4) and the mapping shown in Fig. 3a leads to the solution as follows

$$\begin{aligned} f_\xi(x, y) &= \begin{cases} y & \text{if} \quad x - y > 0 \\ x & \text{if} \quad x - y \leqslant 0 \end{cases} \\ f_R(x, y) &= \begin{cases} k_3(x - y) & \text{if} \quad x - y > 0 \\ 0 & \text{if} \quad x - y \leqslant 0 \end{cases} \end{aligned} \tag{2.5}$$

The graphical solution leading to Eq. $(2.5)_2$ is shown in Fig. 3b where the dashed lines represent two possible locations of the function expressed by Eq. (2.4) for $x - y > 0$ and $x - y < 0$.

2.2.2. DEM simulation

The solution of the above task has been simulated with Yade software. The upper body is modeled as a sphere of radius $r = 0.1\,\mathrm{m}$ and mass $m_I = 4.1888\,\mathrm{kg}$ (resulting from the adopted density of $1000\,\mathrm{kg/m^3}$). The lower body is a flat box of dimensions $0.1\,\mathrm{m}\times0.1\,\mathrm{m}\times0.0001\,\mathrm{m}$ and mass $m_{II} = 0.001\,\mathrm{kg}$. The Zener boundary condition is applied to the box with the following parameters: $c_2 = 1000\,\mathrm{Ns/m}$, $k_1 = k_2 = 10000\,\mathrm{N/m}$. The sphere is initially placed 0.9 m above the box (1.0 m measured to the sphere center), and it falls due to gravity ($g = 10\,\mathrm{m/s^2}$). Contact stiffness, corresponding to k_3 in Fig. 2, equals $10000\,\mathrm{N/m}$ and is independent of the contact penetration u due to the applied linear elastic contact law.

The results of this simulation are compared with the problem formulated analytically in Section 2.2.1 and solved numerically using a Python script.

2.3. Examplary application

This Section presents a more complex simulation to show an examplary application to an engineering problem – a granular layer resting on a viscoelastic foundation. The top of the layer is loaded with a circular steel plate. The simulation resembles a static plate load test often used in the construction process to determine bearing capacity of the granular layer. Nevertheless, the simulation parameters were not calibrated to the field test results. The results are presented for demonstration purposes and qualitative analysis.

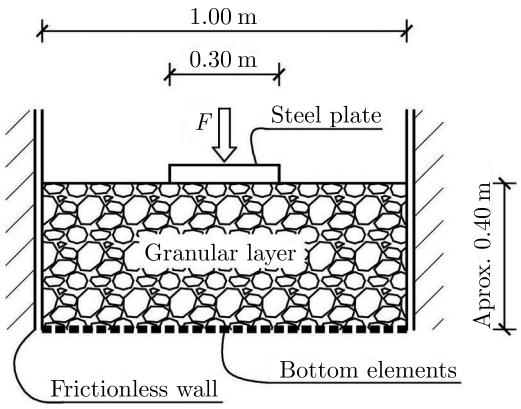

Fig. 4. Problem definition of DEM simulation of plate test

The example, shown in Fig. 4, has been simulated in the following steps:

- Frictionless, rigid, vertical walls were generated to create a vertical funnel with a square cross-section ($1.0\,\mathrm{m}\times1.0\,\mathrm{m}$).
- A discrete bottom boundary condition was created with a layer of small prismatic (box) elements ($0.025\,\mathrm{m}$,$0.025\,\mathrm{m}$,$0.05\,\mathrm{m}$). Hence a layer of 1600 elements was created. At the beginning of simulation, the position of the layer was fixed. However, a permanent vertical force was applied to each box to balance the gravity influence (analogous to geostatic stress often used in geotechnical simulation).
- Loose packing of spherical particles was generated above the bottom layer. Subsequently, the particles fall due to gravity ($g = 10\,\mathrm{m/s^2}$) creating a layer of thickness approximately equal to 0.4 m. The radii of the generated particles ranged between 0.008 m and 0.012 m.
- A steel plate was then placed on top of the granular layer. A cylindrical shape of the plate was achieved by clumping triangular facets into a right prism with twenty joining edges. The mass of the plate was manually prescribed as 10 kg.
- After two seconds (of simulation time), the positions of all bodies were stored as the initial positions. Furthermore, bottom elements remained fixed or were allowed to displace

vertically depending on the scenario. In the second scenario, the vertical movements were constrained by the viscoelastic boundary condition.

- The parameters of constraints applied to each bottom element were computed based on its top wall area. The adopted bedding moduli ($k_{b1} = 20\,\mathrm{N/m^3}$, $k_{b2} = 10\,\mathrm{N/m^3}$, $c_{b2} = 10\,\mathrm{Ns/m^3}$) needed to be multiplied by the top wall area ($0.025 \times 0.025\,\mathrm{m^2}$). Hence, the boundary condition was applied to the bottom element with the following parameters: $k_1 = 12500\,\mathrm{N/m}$, $k_2 = 6250\,\mathrm{N/m}$, $c_2 = 12500\,\mathrm{Ns/m}$.
- Next, the plate was loaded with a linearly increasing vertical force F that reached its maximum value $F_{max} = 17715\,\mathrm{N}$ after 1.78 s and remained constant afterwards. This load was equivalent to stress of 250 kPa since the plate diameter was 0.3 m.
- The particle displacement and reaction forces were stored for further analysis.

The granular layer consisted of only spherical particles. Nevertheless, particle interlocking was achieved by additional rolling resistance. The contact stiffness was controlled by Hertz-Mindlin's (Johnson, 1987) contact law. The remaining material parameters are summarized in Table 1.

Table 1. Material parameters adopted for simulation.

Body type	Density [kg/m^3]	Young's modulus E [GPa]	Poisson's ratio ν [–]	Friction coeff. μ [–]
Spherical particles and bottom elements	2650	1.0	0.25	0.577
Steel plate	7800	210.0	0.25	
Frictionless walls	–	210.0	0.25	0.000

3. Results

3.1. Validation test results

This Section presents a comparison of numerical (DEM) simulation of the soft-contact problem with the solution of its analytical formulation defined in Section 2.2.1. Selected results are presented in Fig. 5.

The output of the simulation reflects phenomena expected in the solution of the simulated problem. The initial position x of the mass m_I equals -0.9 m, and there is no contact force between the two bodies. As soon as the first body (mass m_I) contacts the second one, the contact force shortly increases, pushing the first body back towards its initial position. However, some of the energy is dissipated in the process. Hence, the displacements and the maximum forces during subsequent contact incidents diminish. After approximately 7 s of simulation, the system reaches a static equilibrium, where the elastic reaction resulting from the displacement of the bottom element balances the weight of the upper body. Moreover, the results present a very good agreement between DEM simulation and analytically formulated problems. This shows that both solutions are practically equivalent.

3.2. Results of examplary application

This Section shows the results of two scenarios of plate test simulation. In the first scenario, the bottom elements are fixed in place. Therefore, the foundation is very stiff. However, some deformation is allowed due to the elastic properties of contacts between the spherical particles and bottom elements. In the second scenario, the bottom elements can move vertically. Nevertheless, the movement is constrained by the viscoelastic boundary condition. Figure 6 shows the cross-section of the granular layer at the end of the test.

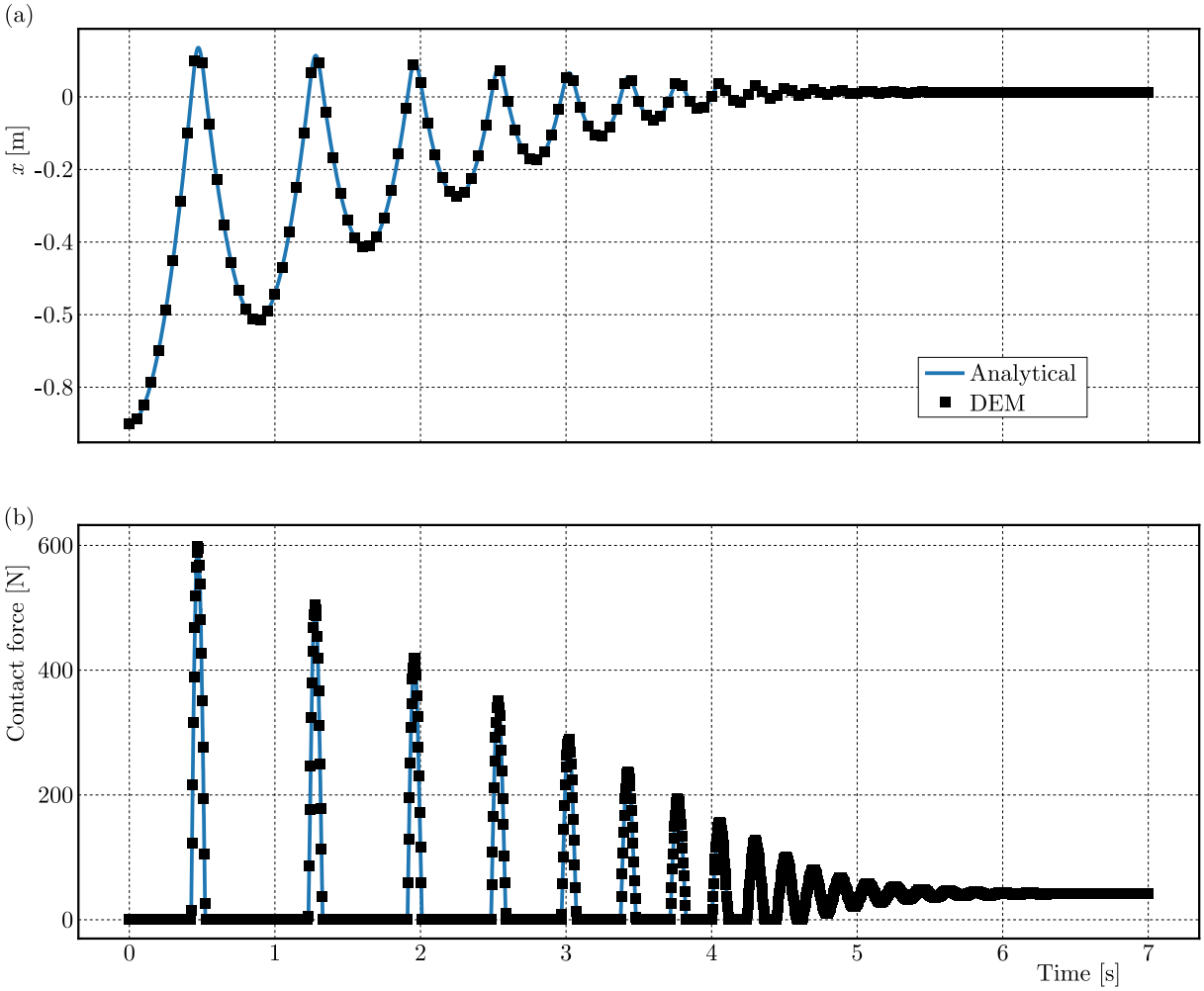

Fig. 5. Results of the soft contact problem solution obtained with an analytical formulation and numerical (DEM) simulation: (a) position of mass m_I, (b) contact force R

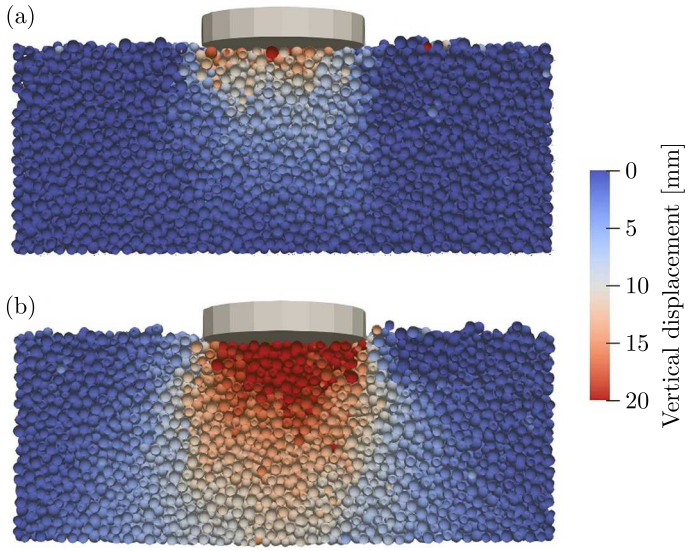

Fig. 6. Displacement of particles in plate test simulation: (a) bottom elements fixed, (b) bottom elements constrained by a viscoelastic boundary condition

In the case of the fixed boundary condition, Fig. 6a, the plate causes only indentation at the top of the layer. This simplified approach can be used to reflect the behavior of the granular material in a relatively stiff container. The results obtained with the viscoelastic boundary condition shown in Fig. 6b resemble displacements of the layer on the deformable foundation (such as an aggregate layer on the soil). This conclusion is also supported by the results presented in Fig. 7.

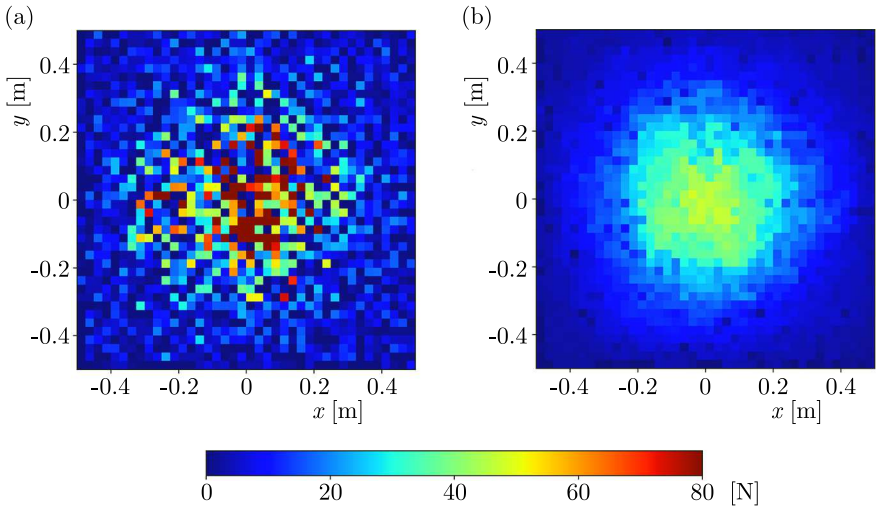

Fig. 7. Distribution of reaction forces acting on bottom elements in plate test simulation: (a) bottom elements fixed, (b) bottom elements constrained by a viscoelastic boundary condition

The reaction force in the deformable foundation is distributed more evenly (see Fig. 7b). There is a distinct circular area of load concentration below the plate that smoothly decreases towards the edges. While in the case of the fixed bottom, the reaction force distribution is much more scattered. Still, the area of the high load is approximately indicated by force concentrations. Nevertheless, the particles at the bottom could not rearrange to redistribute the load on the plate more evenly.

4. Conclusions

This paper presents an implementation of a viscoelastic boundary condition to Yade software. Two simulations have been conducted to demonstrate potential applications of the proposed feature: a one-dimensional soft contact problem and the foundation of a three-dimensional granular layer. The following conclusions can be drawn:

- The implementation works correctly. The results from DEM simulation fit the output of the analytically formulated problem.
- It can be used to simulate foundations, particularly in geotechnical issues, pavement design, compaction simulations, etc.
- The proposed approach allows for realistic yet efficient modeling of foundations purely within the DEM framework.
- The current version is limited to constraining linear displacements of the elements. It can be further developed (e.g. to constrain rotational degrees of freedom).

Acknowledgments

Research was funded by Warsaw University of Technology within the Excellence Initiative: Research University (IDUB) programme.

References

1. Brzeziński K., Gladky A., 2022, Clump breakage algorithm for DEM simulation of crushable aggregates, *Tribology International*, **173**, 107661
2. Chen Y., Jaksa M.B., Kuo Y.-L., Airey D.W., 2021, Investigating the effectiveness of Rolling Dynamic Compaction (RDC) using Discrete Element Method (DEM), *Granular Matter*, **23**, 94, 1-21
3. Cheng H., Yamamoto H., Thoeni K., 2016, Numerical study on stress states and fabric anisotropies in soilbags using the DEM, *Computers and Geotechnics*, **76**, 170-183
4. Cheung G., O'Sullivan C., 2008, Effective simulation of flexible lateral boundaries in two- and three-dimensional DEM simulations, *Particuology*, **6**, 6, 483-500
5. Cundall P.A., Strack O.D.L., 1979, A discrete numerical model for granular assemblies, *Géotechnique*, **29**, 1, 47-65
6. Dejong D., Petuz M., Korswagen A., 1973, *Computer Program, BISAR, Layered Systems under Normal and Tangential Surface Loads*, External Report AMSR-000673, Koninklijke Shell Laboratorium
7. Gladkyy A., Kuna M., 2017, DEM simulation of polyhedral particle cracking using a combined Mohr-Coulomb-Weibull failure criterion, *Granular Matter*, **19**, 3, 1-11
8. Hopman P., 1996, VEROAD: A viscoelastic multilayer computer program, *Transportation Research Record*, **1539**, 1, 72-80
9. Itasca's Particle Flow Code Documentation 7.0., 2021, http://docs.itascacg.com/pfc700/contents.html
10. Jia M., Liu B., Xue J., Ma G., 2021, Coupled three-dimensional discrete element-finite difference simulation of dynamic compaction, *Acta Geotechnica*, **16**, 3, 731-747
11. Johnson K.L., 1987, *Contact Mechanics*, Cambridge University Press
12. Orosz Á., Zwierczyk P.T., 2020, Analysis of the stress state of a railway sleeper using coupled FEM-DEM simulation, *ECMS*, 261-265
13. Pei T., Yang X., 2018, Compaction-induced stress in geosynthetic-reinforced granular base course – A discrete element model, *Journal of Rock Mechanics and Geotechnical Engineering*, **10**, 4, 669-677
14. Puppala A.J., Saride S., Chomtid S., 2009, Experimental and modeling studies of permanent strains of subgrade soils, *Journal of Geotechnical and Geoenvironmental Engineering*, **135**, 10, 1379-1389
15. Quezada J.C., Chazallon C., 2022, Discrete element modelling of hot mix asphalt complex modulus using realistic aggregate shapes, *Road Materials and Pavement Design*, **23**(sup1), 178-195
16. Saad B., Mitri H., Poorooshasb H., 2005, Three-dimensional dynamic analysis of flexible conventional pavement foundation, *Journal of Transportation Engineering*, **131**, 6, 460-469
17. Smilauer V., *et al.*, 2021, *Yade Documentation 3rd ed.*, The Yade Project, https://doi.org/10.5281/zenodo.5705394
18. Stránsky J., 2013, Open source DEM-FEM coupling. Particles III, *Proceedings of the III International Conference on Particle-Based Methods: Fundamentals and Applications*, 46-57
19. Thoeni K., Giacomini A., Lambert C., Sloan S.W., Carter J.P., 2014, A 3D discrete element modelling approach for rockfall analysis with drapery systems, *International Journal of Rock Mechanics and Mining Sciences*, **68**, 107-119
20. Winkler E., 1867, *Vortrge über Eisenbahnbau. Gehalten am königl. böhmischen polytechnischen Landesinstitute in Prag. Erstes Heft: Der Eisenbahn-Oberbau*, H. Dominicus, Prag

21. Zbiciak A., Brzeziński K., Michalczyk R., 2017, Constitutive models of pavement asphaltic layers based on mixture compositions, *Journal of Civil Engineering and Management*, **23**, 3, 378-383

22. Zbiciak A., Kozyra Z., 2015, Dynamic analysis of a soft-contact problem using viscoelastic and fractional-elastic rheological models, *Archives of Civil and Mechanical Engineering*, **15**, 1, 286-291

23. Zbiciak A., Michalczyk R., Brzeziński K., 2019, Time-temperature superposition for viscoelastic materials with application to asphalt-aggregate mixes, *International Journal of Environmental Science and Technology*, **16**, 9, 5059-5064

24. Zhang X., Chen E., Li N., Wang L., Si C., Wang, C., 2022, Micromechanical analysis of the rutting evolution of asphalt pavement under temperature-stress coupling based on the discrete element method, *Construction and Building Materials*, **325**, 126800

25. Zhu X., Qian G., Yu H., Yao D., Shi C., Zhang C., 2022, Evaluation of coarse aggregate movement and contact unbalanced force during asphalt mixture compaction process based on discrete element method, *Construction and Building Materials*, **328**, 127004

Manuscript received December 10, 2022; accepted for print February 3, 2023